ADVANCED OPTICAL MATERIALS
www.advopticalmat.de

Near-Infrared Active Metasurface for Dynamic Polarization Conversion

Pin Chieh Wu, Ruzan Sokhoyan, Ghazaleh Kafaie Shirmanesh, Wen-Hui Cheng, and Harry A. Atwater**

Control of optical polarization is central to harnessing the properties of electromagnetic radiation for many applications, including 3D imaging and quantum computation. However, conventional optical polarizing components are typically bulky and static, that is, fixed in their degree of polarization control. Active metasurfaces have potential for versatile polarization control in a compact form factor by temporally modulating electromagnetic amplitudes and phase between orthogonal electric field components. Here, dynamic control of the polarization state of reflected light from an active metasurface is demonstrated. The metasurface uses indium tin oxide (ITO) as an active element in an array of aluminum nanoantennas operating in the telecom range. Applying an electrical bias between the ITO layer and the back reflector modulates the carrier concentration in ITO at the gate-dielectric/ITO interface, resulting in complex refractive index modulation in the epsilon-near-zero condition. This index modulation alters the degree of excitation of plasmonic modes corresponding to the orthogonal polarization components, leading to polarization modulation. By suitably biasing the metasurface, linearly polarized incident light can be converted to cross-polarized, circularly polarized or elliptically polarized light upon reflection. Dynamic control of the reflected polarization state has potentially wide applications in dynamic wave plates, spatial light modulators, and adaptive wavefront control.

1. Introduction

Light polarization is defined by the orientation of the oscillating electric field for an electromagnetic wave, and plays a vital role in information delivery, imaging, and quantum optics applications.[1,2] An ideal polarization converter can transfer an electromagnetic wave with an undefined polarization state into a well-defined one, including linear and circular polarization states. Traditional approaches for polarization conversion impose different degrees of phase retardation onto two orthogonal linear polarization components via bulky wave plates made of birefringent crystals or polymers. The Faraday and Kerr effects are potential methods for polarization rotation and modulation.[3] However, because of the dispersive behavior of natural materials, complicated structural designs or multilayered films are required to overcome the narrow working bandwidth, making the devices large and inappropriate for integration into optical and optoelectronic devices.

Metasurfaces are ultrathin artificially designed optical scatterers, which introduce abrupt changes to the electromagnetic amplitude and phase of the scattered light within a subwavelength spatial region.[4,5] Their design flexibility enables manipulation of the different constitutive properties of light and has accelerated the development of flat optics and low-profile optoelectronic components such as hyperspectral imaging,[6,7] multifunctional focusing metalens,[8–10] and beam shapers.[11,12] Thus, metasurface optics holds promise for versatile polarization control in a compact form factor by introducing chirality,[13] birefringence,[14] or electromagnetic amplitudes and phase shifts between orthogonal electric field components.[15–17] To date, many metasurface-based polarization converters have been demonstrated in a wide range of frequencies,[18–20] and application areas including polarization imaging,[21,22] entangled photon generation,[23] Stokes parameters detection,[24,25] and holographic displays.[26,27] However, metasurface-based polarization conversion has typically been limited to transformation of a well-defined input polarization state into a single output polarization state. A universal polarization converter, which is capable of realizing multiple polarization states when illuminated by a light with a given polarization state, is highly desirable but has not been realized. Such a universal polarization converter should be able to realize various polarization states (mostly linear, circular, and elliptical polarization) in a single compact device. Universal polarization conversion can be achieved by introducing a concept of an

Prof. P. C. Wu
Department of Photonics
National Cheng Kung University
Tainan 70101, Taiwan
E-mail: pcwu@gs.ncku.edu.tw
Prof. P. C. Wu, Dr. R. Sokhoyan, Dr. G. K. Shirmanesh, Dr. W.-H. Cheng, Prof. H. A. Atwater
Thomas J. Watson Laboratory of Applied Physics
California Institute of Technology
Pasadena, CA 91125, USA
E-mail: haa@caltech.edu
Prof. H. A. Atwater
Kavli Nanoscience Institute
California Institute of Technology
Pasadena, CA 91125, USA
The ORCID identification number(s) for the author(s) of this article can be found under https://doi.org/10.1002/adom.202100230.

DOI: 10.1002/adom.202100230

active metasurface-based polarization converter. Prior research has demonstrated a number of active metasurfaces with diverse optical functions[28–34] (including polarization control) by incorporating an active medium into passive metasurface structures. For example, phase-changed materials, monolayer graphene, liquid crystals, nonlinear materials, etc.[35,36] are commonly used for active spatiotemporal metasurfaces. Prior research has shown that embedding varactor diodes into the metasurface enables the universal polarization synthesis at gigahertz (GHz) frequencies. Importantly, the real-time polarization synthesis can be realized in a programmable fashion.[37] Nevertheless, due to limitations of the active media, previous works have mainly focused on the dynamic polarization control at lower frequencies, such as mid-infrared (MIR) wavelengths,[38,39] terahertz (THz),[40,41] and GHz[42] frequencies. Low-profile universal polarization converter operating at optical frequencies is especially relevant in advanced nanophotonics and quantum applications where the implementation of comprehensive polarization control is of prime importance.[23,43] Recently, Ren et. al. have experimentally demonstrated a reconfigurable metasurface-based polarization converter operating at a wavelength of 820 nm.[44] The demonstrated polarization converter is comprised of a layer of Au inverse structure and an ethyl-red switching polymer layer for light polarization control. Active modulation of the polarization of the transmitted light has been achieved upon introduction of a pump beam; however, only linear-to-elliptical polarization conversion and linear polarization rotation have been obtained. Phase-changed materials like GST have also been incorporated with passive nanostructures for tunable polarization modulation.[45,46] Although promising, the tunability relies on the heating process yielding a relatively low tuning speed in such hybrid GST-metal metasurfaces. Very recently, a tunable all-dielectric metasurface for dynamic polarization tuning at a wavelength of 1535.4 nm was introduced,[47] and uses doped Si structures based on quasi-bound states in the continuum.[47] The active tunability of phase difference between two orthogonal electric field components was attained due to the electro-refractive response of doped silicon under an applied bias voltage. Nevertheless, such a tunable Si metasurface can only access circular and elliptical polarization states when the incident light is linearly polarized so that the electric field is at an angle of 45° with respect to the symmetry axis of the unit cell. In summary, an active metasurface suitable for arbitrary polarization transformation at near-infrared (NIR) wavelengths has not yet been realized.

Here, we demonstrate an active metasurface-based polarization converter, which can achieve three common polarization states, namely, right-hand circularly polarized (RCP), right-hand elliptically polarized and linearly cross-polarized states, when illuminated with a linearly polarized light beam. Our active metasurface-based polarization converter operates at telecom wavelengths. To achieve the polarization state of interest, we use an indium tin oxide (ITO)-based tunable metasurface, which can actively control the amplitudes and relative phases of two orthogonally polarized reflected waves. When biasing the ITO layer with respect to a gate metal, the carrier concentration in ITO at the gate-dielectric/ITO interface is modulated, resulting in a change of the refractive index of around 1 nm-thick active ITO layer. When, due to applied electrical bias, the active ITO layer enters the epsilon-near-zero (ENZ) regime, the interaction between the induced plasmonic modes is altered, leading to the modulation of the polarization state of the reflected light. By suitably biasing the metasurface-based polarization converter, the linearly polarized incident light can be converted to linearly cross-polarized, circularly polarized or elliptically polarized light.

2. Results and Discussion

Figure 1 shows the schematic for our proposed dynamic metasurface polarization converter, which consists of a 150 nm-thick Al back reflector, a 20 nm-thick Al_2O_3/HfO_2 nanolaminate (HAOL) gate dielectric, followed by a 5 nm-thick ITO layer, and an array of Al nanoantennas as the topmost layer. We use the HAOL gate dielectric because of its low leakage current, high breakdown field, and large DC permittivity characteristics.[30,48] To realize polarization modulation, the metasurface needs to support two plasmonic modes, which are coupled to each other. In our case, this is achieved via introducing a reflectarray metasurface building block with an anisotropic Al patch nanoantenna. **Figure 2**a schematically illustrates the metasurface unit element. The detailed physical dimensions of the nanoantennas can be found in the caption of Figure 2a. Figure 2b shows the simulation results of the optimized Al nanoantenna, where two plasmonic modes excited by the incoming plane wave polarized along long or short axis on the patch nanoantenna are observed at a wavelength around 1550 nm. All numerical simulations in this work were carried out using finite difference time domain method (Lumerical FDTD). The dielectric permittivity of ITO is described by the Drude model $\varepsilon_{ITO} = \varepsilon_\infty - \omega_p^2/(\omega^2 + i\omega\Gamma)$, where the plasma frequency is given as $\omega_p^2 = Ne^2/\varepsilon_0 m^*$. Here, ε_∞ is the high frequency permittivity, Γ is the damping constant, N is the carrier density, ε_0 is the dielectric permittivity of vacuum, e is the electron charge, and m^* is the electron effective mass. These constants are defined as $\varepsilon_\infty = 4.2345$, $\Gamma = 1.7588 \times 10^{14}$ (rad s^{-1}),

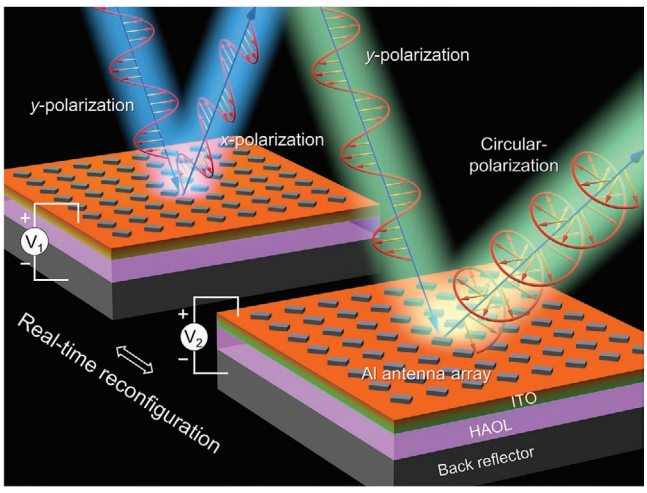

Figure 1. Schematic of the active polarization converter operating in reflection mode. By suitably biasing the metasurface structure, the linearly-polarized incident light can be converted to a cross-polarized, elliptically polarized or circularly polarized light.

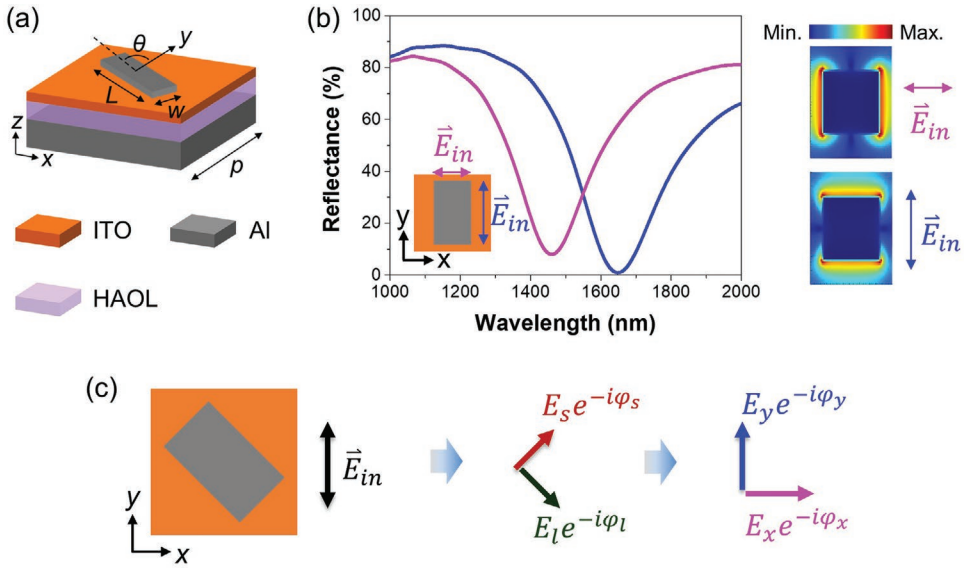

Figure 2. a) Schematic for the tunable metasurface unit cell. The metasurface consists of a 150-nm-thick Al back reflector, a 20-nm-thick HAOL layer, a 5-nm-thick ITO layer, and an array of Al patch nanoantennas with a thickness of 80 nm. The unit cell dimensions are defined as: L = 280 nm, w = 230 nm, and θ = 45°. The periodicity is p = 400 nm. b) Simulated reflectance spectrum of a periodic array of the described unit cell (see the metasurface depicted in Figure 1). Two gap plasmon modes supported by the metasurface are excited when the incident polarization is aligned with the long or short axis of the nanoantenna. c) Design principle of the tunable polarization converter. When a y-polarized light impinges on the metasurface, two gap plasmon modes are excited. The amplitude and phase of the excited modes can be modulated by biasing the ITO layer with respect to the Al mirror.

$N = 2.8 \times 10^{20}$ (cm^{-3}), $m^* = 0.2525m_e$, respectively.[49] When designing the Al nanoantennas, we used the perfectly matched layer (PML) boundary condition in the z direction and the periodic boundary conditions in both x and y directions. The calculations of the reflectance and phase shift of the Al nanoantennas were performed in an array configuration. To numerically calculate the optical response of the tunable metasurface under different electrical biases, we first calculate the spatial distribution of charge density in the ITO layer for different applied bias voltages by using a commercially available software (Lumerical Device), which self-consistently solves Poisson's and the drift-diffusion equations. Once we have calculated the spatial distribution of the carrier density for different applied bias voltages, we use the Drude model to obtain the spatial distribution of the complex dielectric permittivity of ITO, which we incorporate in our full wave optical simulations (Lumerical FDTD). In our electrostatic simulations, the work function of Al and the electron mobility of ITO are taken to be 4.28 eV and 25 $cm^2\ V^{-1}\ s^{-1}$, respectively. The bandgap of ITO and the electron affinity of ITO are set to 2.8 and 4.8 eV, respectively, while the DC permittivity of ITO is taken as 9.3.

In our polarization converter design, we assume that the incident beam is linearly polarized with an electric field E_{in} along the y direction (with 1 V m^{-1} amplitude) such that E_{in} forms a 45° angle with the symmetry axes of the nanoantennas (see Figure 2c). This enables simultaneous excitation of two gap plasmon modes supported by the metasurface (shown in Figure 2b). For the first excited mode, the electric field component along the long side of the nanoantenna is enhanced, while the electric field component along the short side of the nanoantenna is minimized (blue curve and bottom right field profile in Figure 2b). On the other hand, for the second excited mode, the electric field component along the short side of the nanoantenna is enhanced, while the electric field component along the long side of the nanoantenna is minimized (magenta curve and top right field profile in Figure 2b). The x- and y-polarization components of the reflected light beam could be modulated by controlling the interaction between those induced plasmonic modes (see Figure 2c).

Before evaluating the performance of the proposed dynamic polarization converter, we calculate the reflectance and phase of both x- and y-polarized reflected light under different applied biases. Our calculations performed with Lumerical Device software accurately account for the bias-dependent spatial carrier distribution within the ITO layer and the associated spatial variation of the dielectric permittivity. Again, we assume that the incident light is y polarized. **Figure 3**a shows the reflectance of the light beam as a function of wavelength and applied voltage. The top panel of Figure 3a corresponds to the co-polarization reflectance spectrum, while the bottom panel of Figure 3a represents the cross-polarization spectrum under four different applied biases. As seen in Figure 3a, both the x- and y-components of reflected electric field intensity are modulated when electrical bias is present, revealing the ability of amplitude modulation by the proposed tunable metasurface (more results can be found in Figure S1, Supporting Information). Because of the absence of the ENZ condition, the metasurface shows much weaker amplitude modulation under reverse bias (see Figure S2, Supporting Information). It is worth mentioning that the implementation of the active phase shift control also plays a vital role for the realization of a tunable polarization converter. Figure 3b shows the phase difference between x- and y-polarized components of the reflected light as a function of wavelength and applied bias. Here, the phase difference is

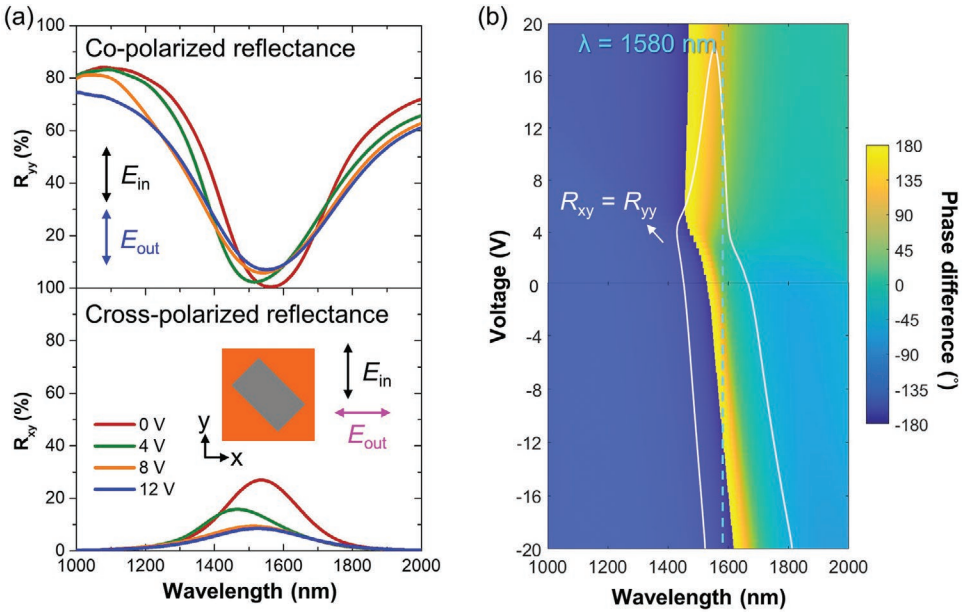

Figure 3. a) Simulated reflectance of the co- (top panel) and cross-polarized (bottom panel) light as a function of wavelength at four different applied voltages. The inset of the bottom panel of (a) shows the orientation of the Al patch nanoantenna with respect to the *x*- and *y*-axis. b) Phase difference between *x*- and *y*-components as a function of wavelength and applied bias. The white solid line marks the parameter values that yield equal reflectance values for *x*- and *y*-polarized components of light.

defined as $\Delta\varphi = \varphi_{yy} - \varphi_{xy}$. Similarly, a significant modulation of the phase difference is observed when the metasurface is forward biased, which is consistent with the amplitude modulation results shown in Figures S1 and S2, Supporting Information.

The realization of circularly polarized reflected light is the most challenging aspect of the tunable polarization converter design. To obtain a circularly polarized light, one needs to confirm that the reflectance values of the *x*- and *y*-polarized light are equal, while the phase difference between the *x*- and *y*-components of the electric field is either 90° or −90°. As shown in Figure 3b, this condition is satisfied at a wavelength of $\lambda = 1580$ nm. Thus, in what follows, we choose the wavelength $\lambda = 1580$ nm as an operating wavelength.

To further explore the physical mechanism behind the observed phase and amplitude modulation, we provide the distributions of the optical electric field in our metasurface-based polarization converter and discuss the change of the near-field coupling conditions at different applied biases. As discussed, the actively tunable amplitude and phase response of the metasurface is achieved by biasing the ITO layer with respect to the Al back reflector. When applying an electrical bias between the ITO layer and the Al back reflector, the carrier density in ITO at the HAOL/ITO interface is modulated, resulting in the change of the refractive index of the ITO layer, as shown in **Figure 4**a. Here, the carrier concentration of ITO at zero applied bias is taken to be 2.8×10^{20} (cm^{-3}).[49] It is worth mentioning that the epsilon-near-zero (ENZ) condition (when the real part of ITO's permittivity is close to zero) is met for gate voltages > ≈3 V (see Figure 4a and Figure S2a, Supporting Information). Thus, we expect to observe a significant optical modulation when the gate bias voltage is larger than 3 V, which is also consistent with the results shown in Figure 3. Figures 4b,c show the *z*-components of the electric field and magnetic field intensities at three different applied biases, respectively. At zero applied bias, a strong near-field coupling between the Al nanoantenna and the back reflector is observed, which results in the strong field confinement within the gate dielectric HAOL layer (the first column in Figure 4b,c). When the metasurface is illuminated by a *y*-polarized light, the emergence of the *z*-component of the electric field in the *xz* plane indicates that we have induced an electric dipole in the patch antenna along x-direction. The coupling between the electric dipole and the image dipole induced in the back reflector leads to a magnetic dipolar resonance with a magnetic moment along y-direction. Remarkably, the E_z component in the *yz* plane shows higher intensity than the one in the *xz* plane, revealing that the polarization component of the reflected light mostly linearly aligns along the *x*-axis. When the voltage is increased to 4 V, the ENZ condition is met. As a result, the optical field is mostly concentrated in the bottom region of the ITO layer (see the middle image of Figure 4b). This asymmetric field profile across the active ITO layer weakens the magnetic energy confinement in the HAOL layer, as shown in the middle image of Figure 4c. Besides, since the E_z component has similar field intensity in the *xz* and *yz* planes, one can anticipate seeing closer *x*- and *y*-polarized reflected light intensity when the bias voltage is 4 V (more details will be discussed in the below). When the applied bias is increased to 14 V, the spatial ITO region in which the ENZ condition is met shifts away from the ITO/HAOL interface (see Figure 4a and the third column in Figure 4b), which further influences the interaction between the Al nanoantenna and the back reflector and makes the magnetic intensity in the HAOL layer weaker (see right image of Figure 4c). Again, when applying an electric bias of 14 V, we can see that in the far field, the intensities of *x* and *y* components of the electric field are very close. This proximity of the far-field values of E_x and E_y is related to the fact that E_z adopts

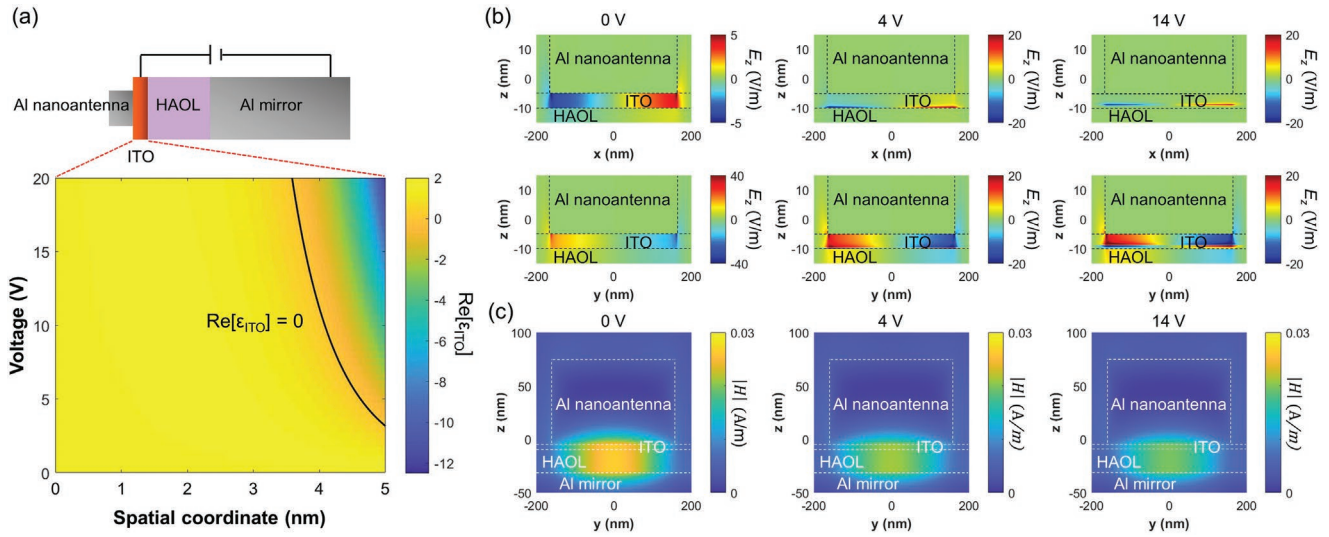

Figure 4. a) Real part of the dielectric permittivity of the 5 nm-thick ITO layer as a function of applied voltage and spatial coordinate. The wavelength is fixed to 1580 nm. b) Spatial distributions of the *z* components of the electric and c) magnetic intensities under different applied biases. Here, the incident light is polarized along *y*-axis and forms a 45° angle with the long side of the patch nanoantennas (see Figure 2c). Because of the onset of the ENZ condition within the active ITO layer, the plasmon coupling between Al nanoantenna and back reflector is tailored, resulting in the amplitude and phase modulations of the reflected light. The wavelength is fixed at 1580 nm. The intensity of incident electric field is 1 V m^{-1}.

very close values the *xz* and *yz* planes. Our analysis shows that we observe a significant modulation of the amplitude, phase, and the polarization state of the reflected light when the active ITO layer undergoes the transition of ENZ condition.

Next, we discuss all the different polarization states that we can access via an active control of the optical response of the metasurface. In our analysis, we assume that the incoming light is *y*-polarized, and the operating wavelength is fixed to $\lambda = 1580$ nm. We decompose the reflected light into the x- and y-polarized components and plot the fraction of the incoming light, which has been converted into each of these components (see **Figure 5**a) as a function of applied bias. Figure 5a also

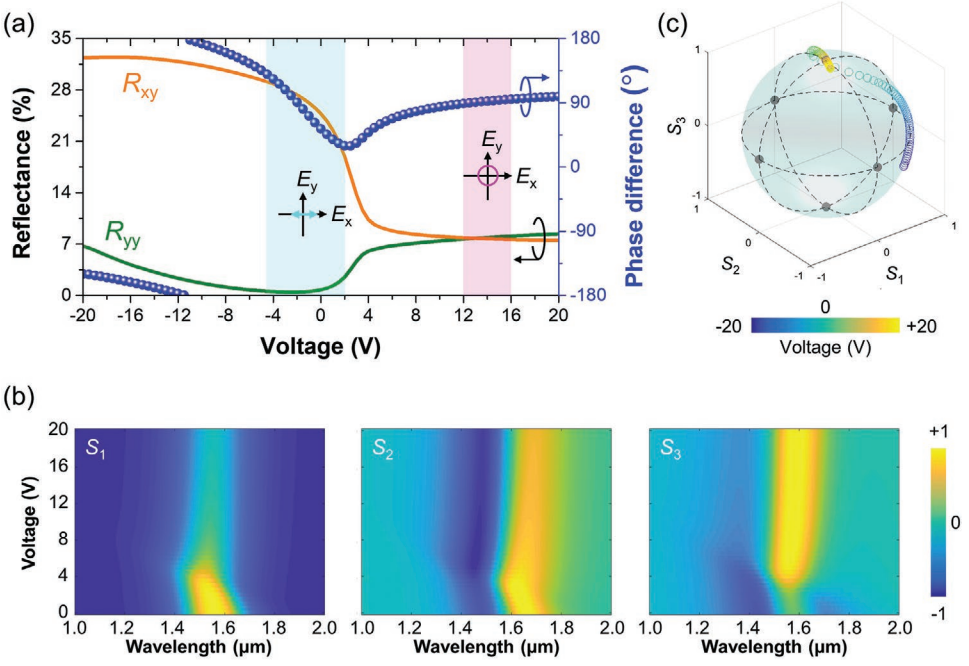

Figure 5. a) Simulated reflectance (orange line: cross-polarized light; olive line: co-polarized light) and phase difference (phase of the co-polarized reflected wave minus the phase of the cross-polarized reflected wave) as a function of applied bias. The metasurface is illuminated by a *y*-polarized normally incident light. The operating wavelength is 1580 nm. The cyan and magenta shadows indicate the range of voltage where the desired polarization states are obtained. b) Plot of the Stokes parameters versus applied electrical bias and wavelength. c) The voltage-dependent path of reflected light polarization state on the Poincaré sphere. Incident wavelength: 1580 nm.

plots the phase difference between the *x*- and *y*-polarized components of the electric field as a function of applied bias. When the applied bias is varied between −4 and 2 V, a y-to-x cross-polarization conversion with about 30% conversion efficiency is realized while the intensity of the y-polarized light is negligible in this voltage range. Here, the linear cross polarization conversion efficiency is defined by the reflectance of the x- polarized component. It is worth mentioning that the thickness of the Al nanoantennas plays a key role in realizing a complete conversion to a linear cross-polarized state (see Figure S11, Supporting Information for more details). As the voltage increases from 2 to ≈12 V, our metasurface realizes a linear-to-elliptical polarization conversion. For the bias voltage range between 12 and 16 V, our metasurface converts the incoming linearly polarized light into a circularly polarized light. A RCP can be realized because we have been able to achieve 90° phase difference between the *x*- and *y*-polarized components of the reflected light when the amplitudes of these components are equal. Since the x- and y-polarized reflectance are equal for a circularly polarized light, the linear-to-circular polarization conversion efficiency can be evaluated by the reflectance of either x-or y-polarized component. As seen in Figure 5a, our tunable metasurface presents ≈8% linear-to-circular polarization conversion efficiency. A possible route to higher polarization conversion efficiency would be using a nanophotonic design, which is similar to the one described in the current work, but replacing the metallic components with high-index dielectric materials. In principle, all-dielectric metasurface can be interfaced with an ITO layer to achieve an electrically tunable optical response. Prior research has investigated a similar approach for realization of the polarization conversion.[50] However, the photonic design used in the mentioned work did not enable the generation of versatile polarization states at a given operating wavelength. One can also design a metasurface comprised of a dielectric electro-optics material,[28] and use the designed metasurface for the polarization conversion. To further evaluate the optical performance, we use the Stokes parameters to investigate the generated polarization state under different applied biases. For an electromagnetic wave propagating along the *z*-axis, the Stokes parameters can be determined by:[24,25]

$$S_0 = |r_x|^2 + |r_y|^2 = R_{xy} + R_{yy} \quad (1)$$

$$S_1 = |r_x|^2 - |r_y|^2 = R_{xy} - R_{yy} \quad (2)$$

$$S_2 = 2|r_x||r_y|\cos(\Delta\varphi) = |r_{45^\circ}|^2 - |r_{-45^\circ}|^2 = R_{45^\circ} - R_{-45^\circ} \quad (3)$$

$$S_3 = 2|r_x||r_y|\sin(\Delta\varphi) = |r_{RCP}|^2 - |r_{LCP}|^2 = R_{RCP} - R_{LCP} \quad (4)$$

where r_x, r_y, r_{45°, r_{-45°, are the complex reflection coefficients of the linearly polarized light with the electric field along the *x*-axis, *y*-axis, at an angle of 45°, and −45° with respect to the *y*-axis, respectively. r_{RCP}, r_{LCP} are the complex reflection coefficients of the light with RCP and left-hand circular polarization (LCP), respectively. $\Delta\varphi = \varphi_{yy} - \varphi_{xy}$ is the phase difference between *x*- and *y*-components of the reflected light, which can be extracted from Figure 3b. Based on the results shown in Figure 5a, we can achieve all three desired polarization states (linear, elliptical, and circular) upon application of a forward bias. Thus, in what follows, we will discuss the case of positive voltages only. Figure 5b plots the calculated Stokes parameters (normalized to S_0) as a function of wavelength and applied bias. As seen in Figure 5b, the calculated Stokes parameters (especially S_1 and S_3) are strongly modulated in the voltage range (3.5, 4.5 V). While for applied biases below 4 V our metasurface converts the linearly polarized light into a linearly cross-polarized light (along the *x*-axis), at an applied of ≈4 V our metasurface realizes linear-to-elliptical polarization conversion. It is also consistent with the aforementioned points: the active ITO layer enters the ENZ region when the applied bias voltage is >≈3 V. It is worth noting that S_1 and S_2 are close to zero while S_3 is almost unity when the voltage is within the (12, 16 V) range, which further confirms that our metasurface coverts the incoming linearly polarized light into a circularly polarized light of high purity.

To clearly describe the dynamics of the polarization state of the reflected light, we plot the voltage-dependent path of the polarization states on the Poincaré sphere (Figure 5c). In Figure 5c, the operating wavelength 1580 nm. First, we can see that the incident *y*-polarized light is converted to an almost *x*-polarized light at 0 V. The polarization state moves towards the upper hemisphere corresponding to the right-hand elliptical polarization when electrical bias is increased, and resides around the north-pole, corresponding to the RCP, when the bias voltage keeps increasing. On the other hand, the polarization state moves towards the lower hemisphere, corresponding to the left-hand elliptical polarization, when a negative voltage is applied. Thus, our dynamic polarization converter enables the conversion of the linearly-polarized incident light into a cross-polarized, circularly-polarized, or elliptically-polarized reflected wave, three widely used polarization states, by suitably biasing the metasurface.

Moreover, the proposed metasurface is capable of accessing other polarization states on the Poincaré sphere at different operating wavelengths (see Figure S3, Supporting Information). For example, at an operating wavelength of 1456 nm, we can actively covert the polarization state of the reflected light from a left-hand elliptical polarization to a linear polarization with an electric field at an angle of −45° with respect to *y*-axis. The described elliptical-to-linear polarization conversion occurs when we increase the bias voltage from 0 to 6 V. The polarization state becomes a left-hand elliptical polarization again when the voltage is further increased. In addition, an LCP can be realized at a wavelength of 1456 nm when a negative bias voltage is applied. Interestingly, at an operating wavelength of 1632 nm, we can actively switch between a linearly polarized light (with an *x*-polarization) to a right-hand elliptically polarized light, and a linearly polarized light with an electric field at an angle of +45° with respect to *y*-axis (see Figure S3, Supporting Information).

3. Conclusion

In conclusion, we propose an actively tunable metasurface polarization converter, which is based on a field effect-induced modulation of the properties of the ITO layer. When applying

an electrical bias between the active ITO layer and the back reflector, the carrier concentration at the gate-dielectric/ITO interface is modulated, resulting in a change of the complex refractive index of the ITO layer. The introduction of the ENZ condition enables altering the interaction between the induced plasmonic modes, leading to the modulation of the polarization state of the reflected light. Our analysis shows that the optimization of the optical parameters of the ITO layer and the structural dimensions of metasurface polarization converter is crucial for achieving a significant change in the polarization state of the reflected light. Indeed, in our experiments, we have been able to observe only linear to elliptical polarization conversion because of an imperfect match of the properties of the ITO layer and the structural parameters of the metasurface (see Part 3 of Supporting Information). However, our simulation results show that for given properties of the ITO layer, we can suitably adjust the structural parameters of the metasurface to ensure generation of versatile polarization states when the metasurface is suitably biased (for further details see Part 3 of Supporting Information). By suitably biasing the metasurface structure, the proposed polarization converter can actively transform the incoming linearly *y*-polarized light into a linearly cross-polarized, circularly-polarized, or elliptically-polarized reflected light at telecom wavelengths, depending on an applied voltage. We estimate that the modulation frequency of the proposed metasurface polarization converter is on the order of MHz.[49,51] The modulation frequency could reach a GHz range if the RC time constant is minimized via an appropriate electrical interconnect design.[52] Finally, we would like to mention that the wavelength of the ENZ condition can be significantly shifted by tuning the atomic ratio of the metal in the metal-ITO co-sputtered films.[53] It has been previously shown that metal-ITO composite films may exhibit an ENZ transition at shorter wavelengths as compared with the pure ITO films once the composite films have been annealed.[53] While the thickness of the demonstrated metal-ITO composite films is 200 nm, the thickness of the ITO layer in our tunable polarizer is only 5 nm. If it were possible to fabricate much thinner metal-ITO composite films with a blue-shifted ENZ region than, in principle, the operating wavelength of the tunable polarizer could be significantly blue-shifted. This dynamic control of the amplitude, phase as well as the polarization state of the reflected light provides prospects for various applications, such as dynamic wave plates, low-profile spatial light modulators, adaptive wavefront control, signal monitoring and detection, and quantum optics. As we have discussed, ITO may be used as an electrically controlled material in active metasurfaces or metamaterials operating in the NIR wavelength range. This is because the ENZ region of ITO can be dynamically shifted under applied electrical bias. It is worth mentioning that ITO is also an attractive material for the stealth and communication integration technology since it exhibits a diverse optical response in different parts of the electromagnetic spectrum.[54] For the stealth applications, it is essential to introduce a material, that which exhibits low thermal emissivity in the infrared (IR) region of the electromagnetic spectrum (specifically, 8–14 μm).[54] According to the Kirchhoff's law, the low thermal emissivity can be obtained when a material, which highly reflective in IR is used. Both metals and ITO are highly reflective in the IR wavelength range.[55] Unlike metals, however, ITO exhibits optical transparency, which is required for stealth applications. Prior research has also shown that an ITO-based heterostructure can exhibit a transparency window in the microwave wavelength region, which makes ITO a promising material for the communication-compatible multispectral stealth technology. To conclude, we believe that ITO is a promising material for diverse optical applications due to its versatile optical response in different parts of the electromagnetic spectrum.

Supporting Information

Supporting Information is available from the Wiley Online Library or from the author.

Acknowledgements

This work was supported by the Air Force Office of Scientific Research under Grant FA9550-19-1-0279. The authors used facilities supported by the Kavli Nanoscience Institute (KNI). P.C.W. acknowledges the support from Ministry of Science and Technology, Taiwan (Grant numbers: 108-2112-M-006-021-MY3; 107-2923-M-006-004-MY3) and the support in part by Higher Education Sprout Project, Ministry of Education to the Headquarters of University Advancement at National Cheng Kung University (NCKU). P.C.W. also acknowledges the support from Ministry of Education (Yushan Young Scholar Program), Taiwan.

Conflict of Interest

The authors declare no conflict of interest.

Data Availability Statement

Research data are not shared.

Keywords

active control, metasurfaces, nanophotonics, polarization converter, tunable polarizer

Received: February 2, 2021
Revised: May 1, 2021
Published online:

[1] D. Singh, *Fundamentals of Optics*, 2nd Ed., Prentice Hall India Pvt., Ltd, New Delhi **2015**.
[2] R. Shankar, *Fundamentals of Physics II: Electromagnetism, Optics, and Quantum Mechanics*, Yale University Press, London **2016**.
[3] S. Vandendriessche, S. Van Cleuvenbergen, P. Willot, G. Hennrich, M. Srebro, V. K. Valev, G. Koeckelberghs, K. Clays, J. Autschbach, T. Verbiest, *Chem. Mater.* **2013**, *25*, 1139.
[4] S. Sun, Q. He, J. Hao, S. Xiao, L. Zhou, *Adv. Opt. Photon.* **2019**, *11*, 380.
[5] X. Luo, *ACS Photonics* **2018**, *5*, 4724.
[6] M. Faraji-Dana, E. Arbabi, H. Kwon, S. M. Kamali, A. Arbabi, J. G. Bartholomew, A. Faraon, *ACS Photonics* **2019**, *6*, 2161.

[7] F. Yesilkoy, E. R. Arvelo, Y. Jahani, M. Liu, A. Tittl, V. Cevher, Y. Kivshar, H. Altug, *Nat. Photonics* **2019**, *13*, 390.
[8] M. Khorasaninejad, W. T. Chen, A. Y. Zhu, J. Oh, R. C. Devlin, D. Rousso, F. Capasso, *Nano Lett.* **2016**, *16*, 4595.
[9] B. H. Chen, P. C. Wu, V.-C. Su, Y.-C. Lai, C. H. Chu, I. C. Lee, J.-W. Chen, Y. H. Chen, Y.-C. Lan, C.-H. Kuan, D. P. Tsai, *Nano Lett.* **2017**, *17*, 6345.
[10] Q. Guo, Z. Shi, Y.-W. Huang, E. Alexander, C.-W. Qiu, F. Capasso, T. Zickler, *Proc. Nat. Aca. Sci. USA* **2019**, *116*, 22959.
[11] Y.-Y. Xie, P.-N. Ni, Q.-H. Wang, Q. Kan, G. Briere, P.-P. Chen, Z.-Z. Zhao, A. Delga, H.-R. Ren, H.-D. Chen, C. Xu, P. Genevet, *Nat. Nanotechnol.* **2020**, *15*, 125.
[12] H. Sroor, Y.-W. Huang, B. Sephton, D. Naidoo, A. Vallés, V. Ginis, C.-W. Qiu, A. Ambrosio, F. Capasso, A. Forbes, *Nat. Photonics* **2020**, *14*, 498.
[13] P. Yu, J. Li, C. Tang, H. Cheng, Z. Liu, Z. Li, Z. Liu, C. Gu, J. Li, S. Chen, J. Tian, *Light Sci. Appl.* **2016**, *5*, e16096.
[14] Z. Shi, A. Y. Zhu, Z. Li, Y.-W. Huang, W. T. Chen, C.-W. Qiu, F. Capasso, *Sci. Adv.* **2020**, *6*, eaba3367.
[15] P. C. Wu, W.-Y. Tsai, W. T. Chen, Y.-W. Huang, T.-Y. Chen, J.-W. Chen, C. Y. Liao, C. H. Chu, G. Sun, D. P. Tsai, *Nano Lett.* **2017**, *17*, 445.
[16] P. C. Wu, W. Zhu, Z. X. Shen, P. H. J. Chong, W. Ser, D. P. Tsai, A.-Q. Liu, *Adv. Opt. Mater.* **2017**, *5*, 1600938.
[17] Z. Wu, Y. Ra'di, A. Grbic, *Phys. Rev. X* **2019**, *9*, 011036.
[18] M. Kamali Seyedeh, E. Arbabi, A. Arbabi, A. Faraon, *Nanophotonics* **2018**, *7*, 1041.
[19] C. Hou-Tong, J. T. Antoinette, Y. Nanfang, *Rep. Prog. Phys.* **2016**, *79*, 076401.
[20] H. Yueqiang, W. Xudong, L. Xuhao, O. Xiangnian, L. Ling, C. Yiqin, Y. Ping, W. Shuai, D. Huigao, *Nanophotonics* **2020**, *9*, 3755.
[21] I. S. Osborne, *Science* **2019**, *365*, 40.
[22] E. Arbabi, S. M. Kamali, A. Arbabi, A. Faraon, *ACS Photonics* **2018**, *5*, 3132.
[23] T. Stav, A. Faerman, E. Maguid, D. Oren, V. Kleiner, E. Hasman, M. Segev, *Science* **2018**, *361*, 1101.
[24] A. Pors, M. G. Nielsen, S. I. Bozhevolnyi, *Optica* **2015**, *2*, 716.
[25] P. C. Wu, J.-W. Chen, C.-W. Yin, Y.-C. Lai, T. L. Chung, C. Y. Liao, B. H. Chen, K.-W. Lee, C.-J. Chuang, C.-M. Wang, D. P. Tsai, *ACS Photonics* **2018**, *5*, 2568.
[26] L. Jin, Z. Dong, S. Mei, Y. F. Yu, Z. Wei, Z. Pan, S. D. Rezaei, X. Li, A. I. Kuznetsov, Y. S. Kivshar, J. K. W. Yang, C.-W. Qiu, *Nano Lett.* **2018**, *18*, 8016.
[27] R. Zhao, B. Sain, Q. Wei, C. Tang, X. Li, T. Weiss, L. Huang, Y. Wang, T. Zentgraf, *Light Sci. Appl.* **2018**, *7*, 95.
[28] P. C. Wu, R. A. Pala, G. Kafaie Shirmanesh, W.-H. Cheng, R. Sokhoyan, M. Grajower, M. Z. Alam, D. Lee, H. A. Atwater, *Nat. Commun.* **2019**, *10*, 3654.
[29] Y. Kim, P. C. Wu, R. Sokhoyan, K. Mauser, R. Glaudell, G. Kafaie Shirmanesh, H. A. Atwater, *Nano Lett.* **2019**, *19*, 3961.
[30] G. Kafaie Shirmanesh, R. Sokhoyan, R. A. Pala, H. A. Atwater, *Nano Lett.* **2018**, *18*, 2957.
[31] L. B. Yan, W. M. Zhu, P. C. Wu, H. Cai, Y. D. Gu, L. K. Chin, Z. X. Shen, P. H. J. Chong, Z. C. Yang, W. Ser, D. P. Tsai, A. Q. Liu, *Appl. Phys. Lett.* **2017**, *110*, 201904.
[32] G. K. Shirmanesh, R. Sokhoyan, P. C. Wu, H. A. Atwater, *ACS Nano* **2020**, *14*, 6912.
[33] A. L. Holsteen, A. F. Cihan, M. L. Brongersma, *Science* **2019**, *365*, 257.
[34] C. Zhang, S. Xiao, Y. Wang, Y. Gao, Y. Fan, C. Huang, N. Zhang, W. Yang, Q. Song, *Laser Photon. Rev.* **2019**, *13*, 1900079.
[35] L. Kang, R. P. Jenkins, D. H. Werner, *Adv. Opt. Mater.* **2019**, *7*, 1801813.
[36] A. M. Shaltout, V. M. Shalaev, M. L. Brongersma, *Science* **2019**, *364*, eaat3100.
[37] J. C. Ke, J. Y. Dai, M. Z. Chen, L. Wang, C. Zhang, W. Tang, J. Yang, W. Liu, X. Li, Y. Lu, Q. Cheng, S. Jin, T. J. Cui, *Small Struct.* **2021**, *2*, 2000060.
[38] J. Li, P. Yu, H. Cheng, W. Liu, Z. Li, B. Xie, S. Chen, J. Tian, *Adv. Opt. Mater.* **2016**, *4*, 91.
[39] H. Cheng, S. Chen, P. Yu, J. Li, B. Xie, Z. Li, J. Tian, *Appl. Phys. Lett.* **2013**, 103.
[40] L. Cong, N. Xu, J. Gu, R. Singh, J. Han, W. Zhang, *Laser Photon. Rev.* **2014**, *8*, 626.
[41] R.-H. Fan, Y. Zhou, X.-P. Ren, R.-W. Peng, S.-C. Jiang, D.-H. Xu, X. Xiong, X.-R. Huang, M. Wang, *Adv. Mater.* **2015**, *27*, 1201.
[42] W. Li, S. Xia, B. He, J. Chen, H. Shi, A. Zhang, Z. Li, Z. Xu, *IEEE T. Antenn. Propag.* **2016**, *64*, 5281.
[43] Z.-K. Zhou, J. Liu, Y. Bao, L. Wu, C. E. Png, X.-H. Wang, C.-W. Qiu, *Prog. Quantum Electron.* **2019**, *65*, 1.
[44] M.-X. Ren, W. Wu, W. Cai, B. Pi, X.-Z. Zhang, J.-J. Xu, *Light Sci. Appl.* **2017**, *6*, e16254.
[45] M. Wuttig, H. Bhaskaran, T. Taubner, *Nat. Photonics* **2017**, *11*, 465.
[46] S. Abdollahramezani, O. Hemmatyar, H. Taghinejad, A. Krasnok, Y. Kiarashinejad, M. Zandehshahvar, A. Alù, A. Adibi, *Nanophotonics* **2020**, *9*, 1189.
[47] M. M. Salary, H. Mosallaei, *ACS Photonics* **2020**, *7*, 1813.
[48] G. K. Shirmanesh, R. Sokhoyan, P. C. Wu, H. A. Atwater, *ACS Nano* **2020**, *14*, 6912.
[49] Y.-W. Huang, H. W. H. Lee, R. Sokhoyan, R. A. Pala, K. Thyagarajan, S. Han, D. P. Tsai, H. A. Atwater, *Nano Lett.* **2016**, *16*, 5319.
[50] A. Forouzmand, M. M. Salary, S. Inampudi, H. Mosallaei, *Adv. Opt. Mater.* **2018**, *6*, 1701275.
[51] Y. Lee, J. Yun, S.-J. Kim, M. Seo, S. In, H.-D. Jeong, S.-Y. Lee, N. Park, T. D. Chung, B. Lee, *Adv. Opt. Mater.* **2020**, *8*, 2001256.
[52] A. Forouzmand, M. M. Salary, G. Kafaie Shirmanesh, R. Sokhoyan, H. A. Atwater, H. Mosallaei, *Nanophotonics* **2019**, *8*, 415.
[53] C. Chen, Z. Wang, K. Wu, H. Ye, *Sci. Technol. Adv. Mater.* **2018**, *19*, 174.
[54] C. Zhang, J. Yang, W. Yuan, J. Zhao, J. Y. Dai, T. C. Guo, J. Liang, G. Y. Xu, Q. Cheng, T. J. Cui, *J. Phys. D: Appl. Phys.* **2017**, *50*, 444002.
[55] S. Zhong, L. Wu, T. Liu, J. Huang, W. Jiang, Y. Ma, *Opt. Express* **2018**, *26*, 16466.